Supporting Information

Spinel Zinc Manganate-based High-Capacity and High-Stability Non-Aqueous Zinc-Ion Battery

Prakash Kumar Pathak,[a] *Nitish Kumar,*[a] *Heejoon Ahn,*[b] *Rahul R. Salunkhe*[a]*

[a]Department of Physics, Indian Institute of Technology Jammu, Jammu and Kashmir, 181221, India.

[b]Human-Tech Convergence Program, Department of Organic and Nano Engineering, Hanyang University, 222 Wangshimni-ro, Seongdong-gu, Seoul 04763, Republic of Korea.

*E-mail: rahul.salunkhe@iitjammu.ac.in

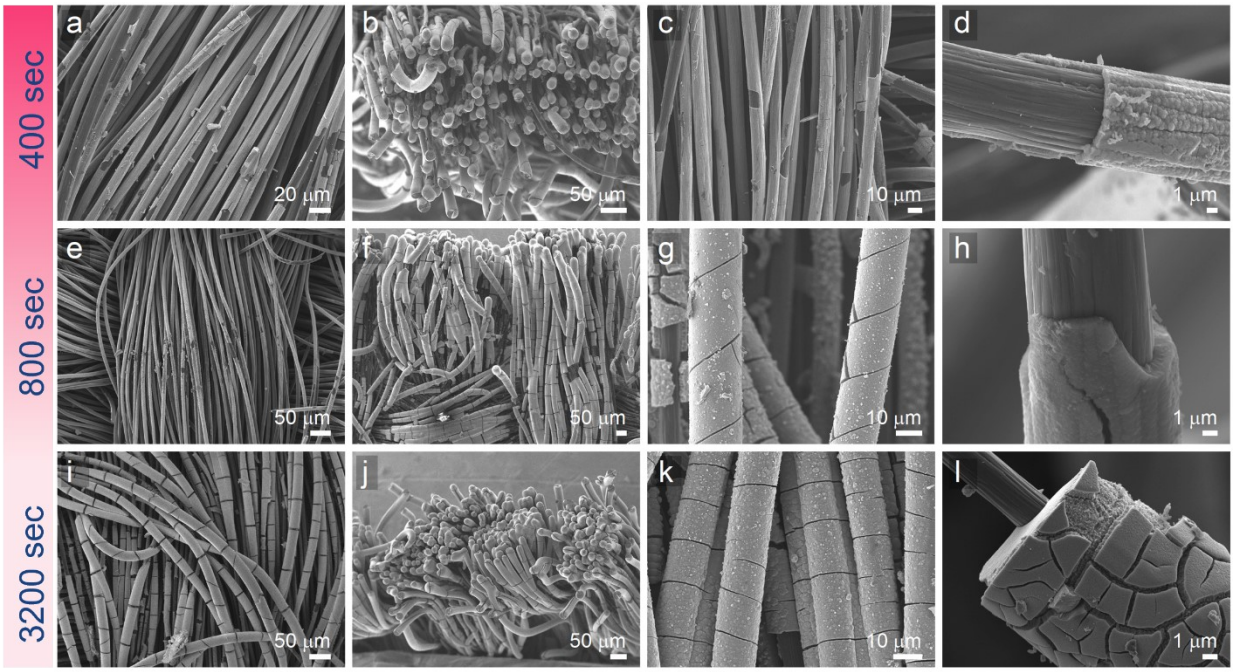

Figure S1. ZMC with different electrodeposition times. Low and high magnification images of (a-d) ZMC-4 (400 sec), (e-h) ZMC-8 (800 sec), (i-l) ZMC-32 (3200 sec). (b), (f) and (j) show the cross-sectional FESEM image of ZMC-4, ZMC-8 & and ZMC-32, respectively.

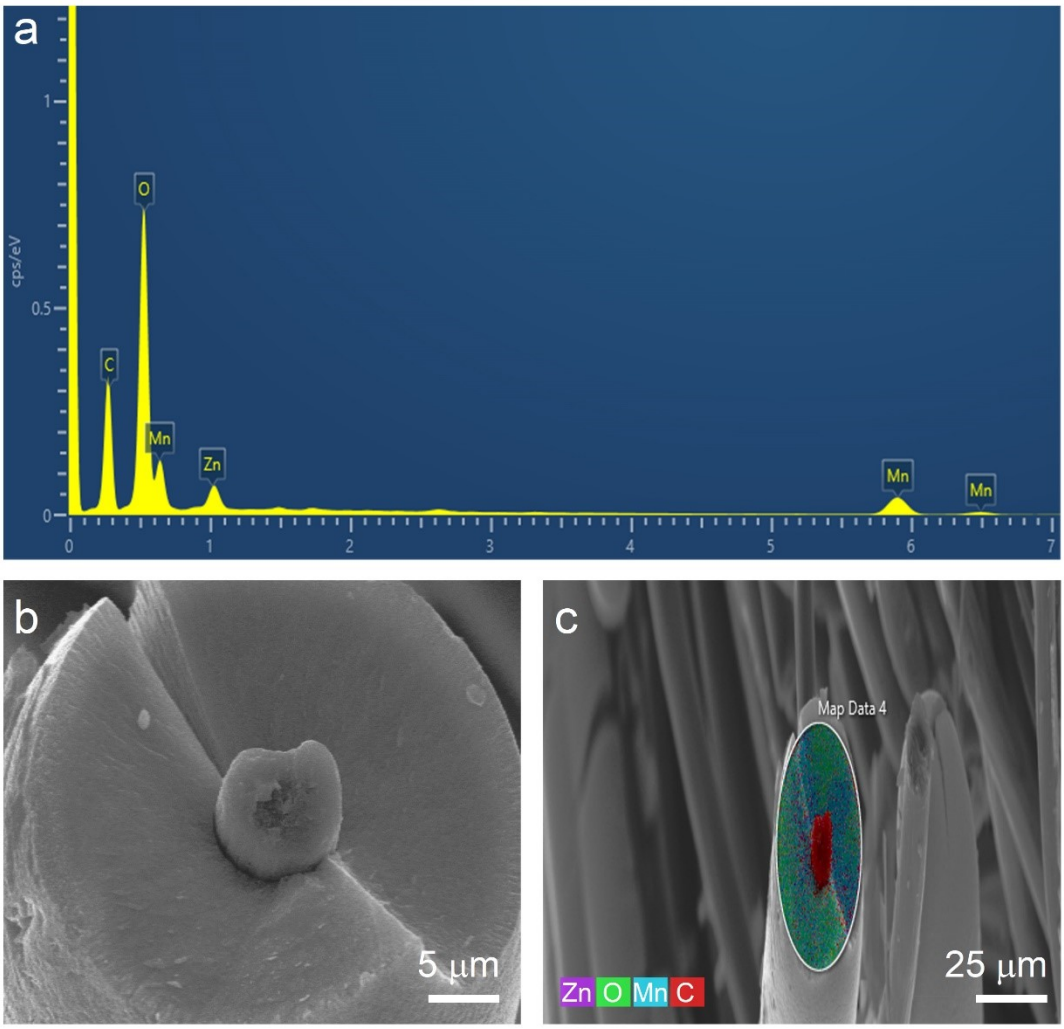

Figure S2. (a) EDS spectra of ZMC-32 (b) cross-sectional FESEM image with (c) overlapped EDS image of ZMC-32.

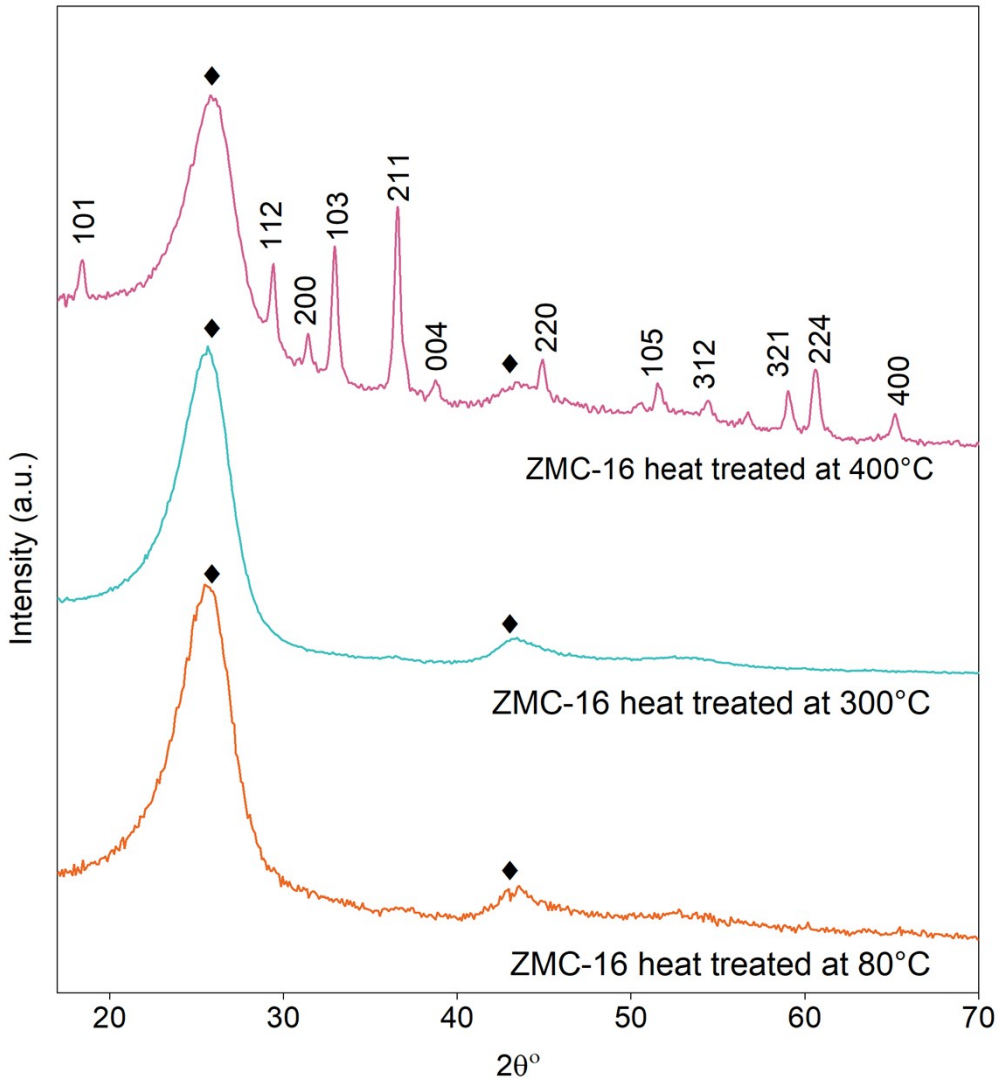

Figure S3. XRD pattern of ZMC-16 at various temperature conditions 80 ℃, 300 ℃, and 400 ℃. The crystalline phase was observed after heat treatment of 400 ℃. The asterisk mark indicates the peak occurred due to carbon cloth.

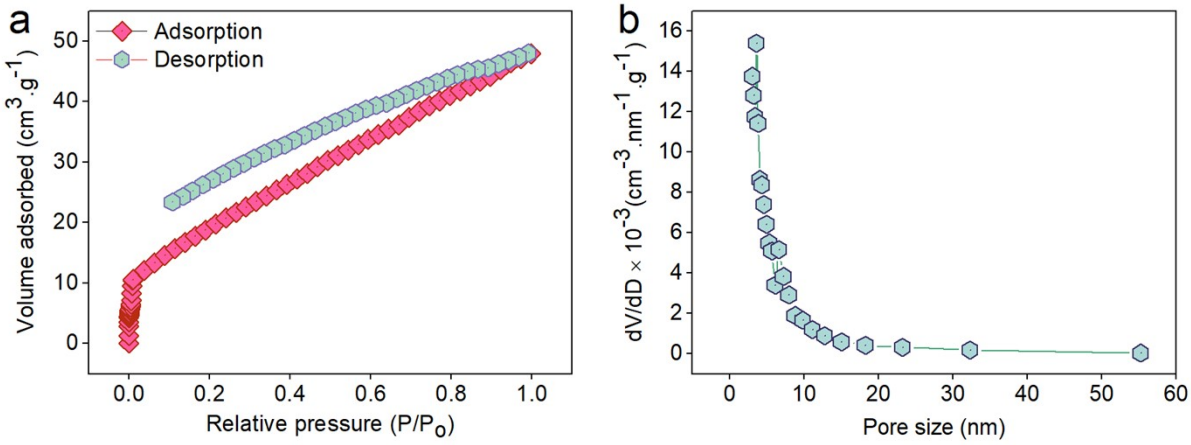

Figure S4. (a) Adsorption–desorption isotherms for the ZMC-16 sample at 77 K, and (f) BJH model pore size distribution of the same sample.

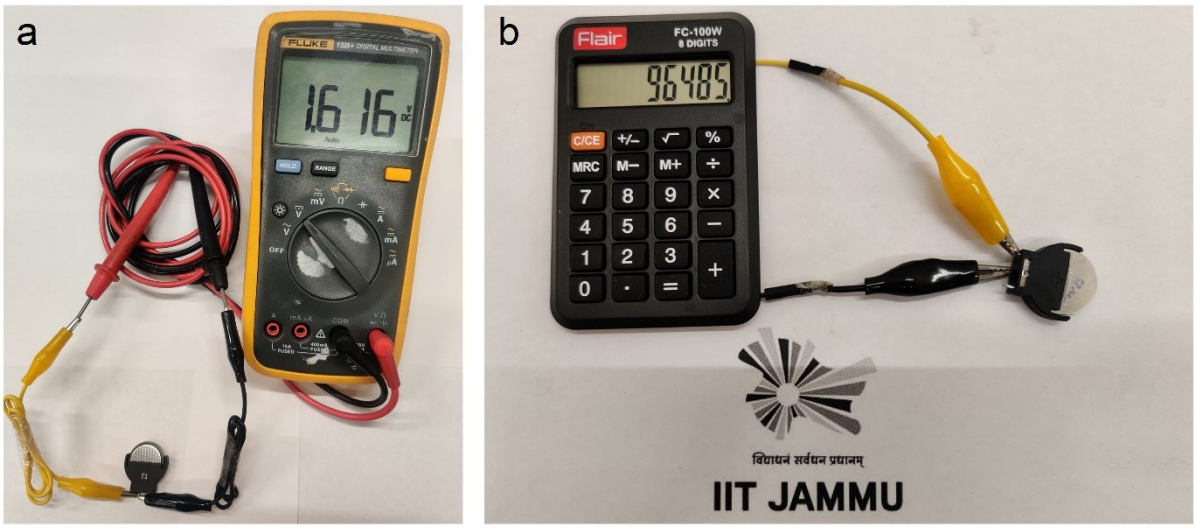

Figure S5. (a) Open circuit voltage of Zn//ZMC-16 measured after the cell has reached equilibrium, (b) a calculator being operated powered by ZMC ZIB.

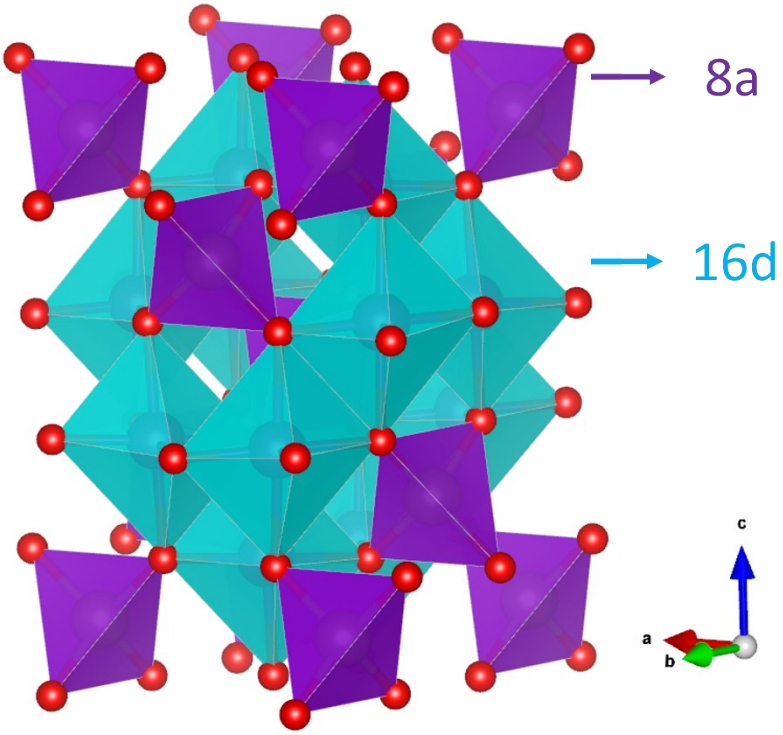

Figure S6: $ZnMn_2O_4$ crystal structure with 8a tetrahedra shown in purple, 16d octahedra shown in cyan, oxygen atoms are indicated by red colour.

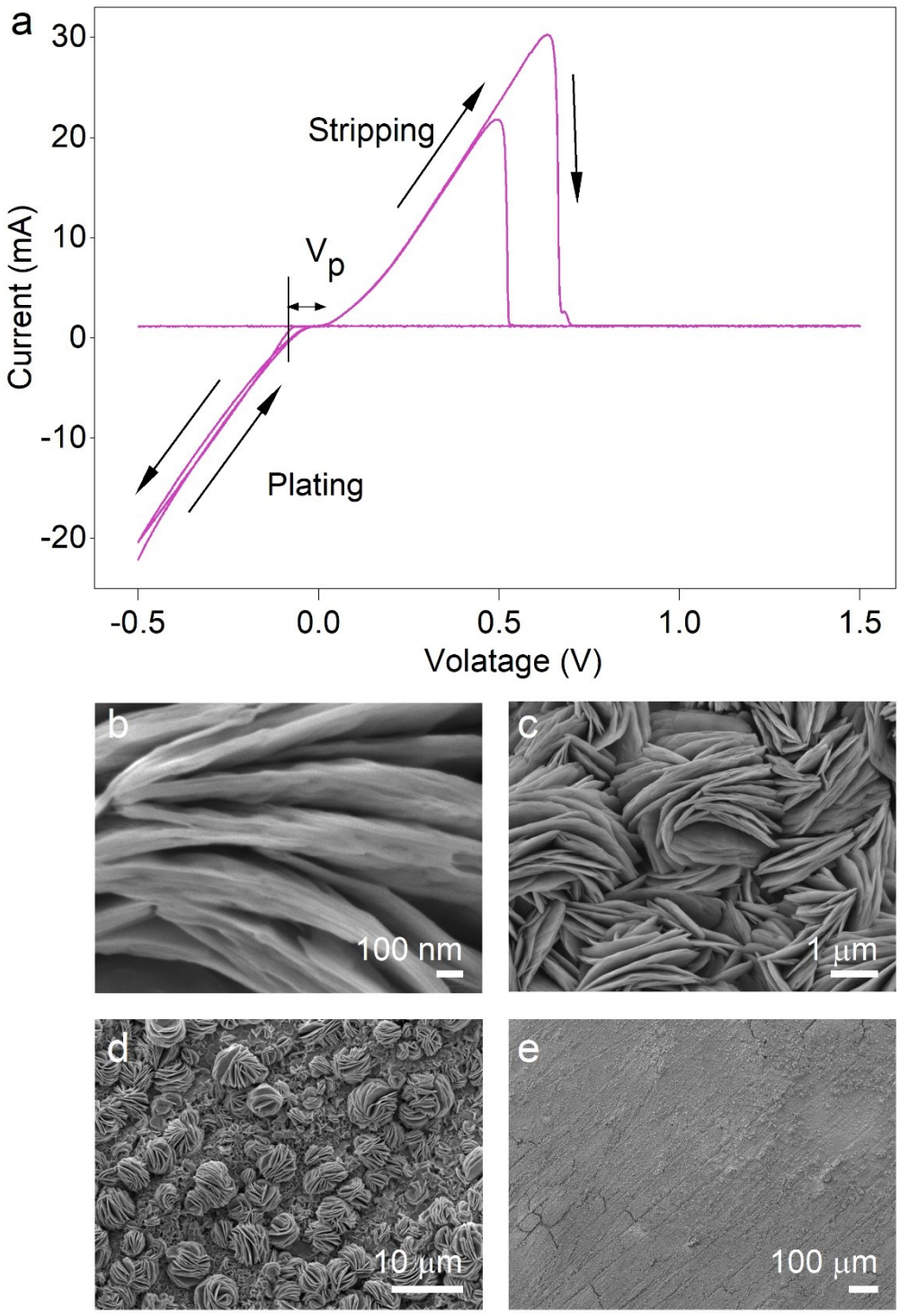

Figure S7. Stripping and plating study of zinc anode in 0.5 M $ZnClO_4$ acetonitrile and corresponding FESEM images (a) CV curve in the voltage range of -0.5 V to 1.5 V at 5 mV s^{-1} (b-e) FESEM image of zinc foil at various magnifications after stripping and plating.

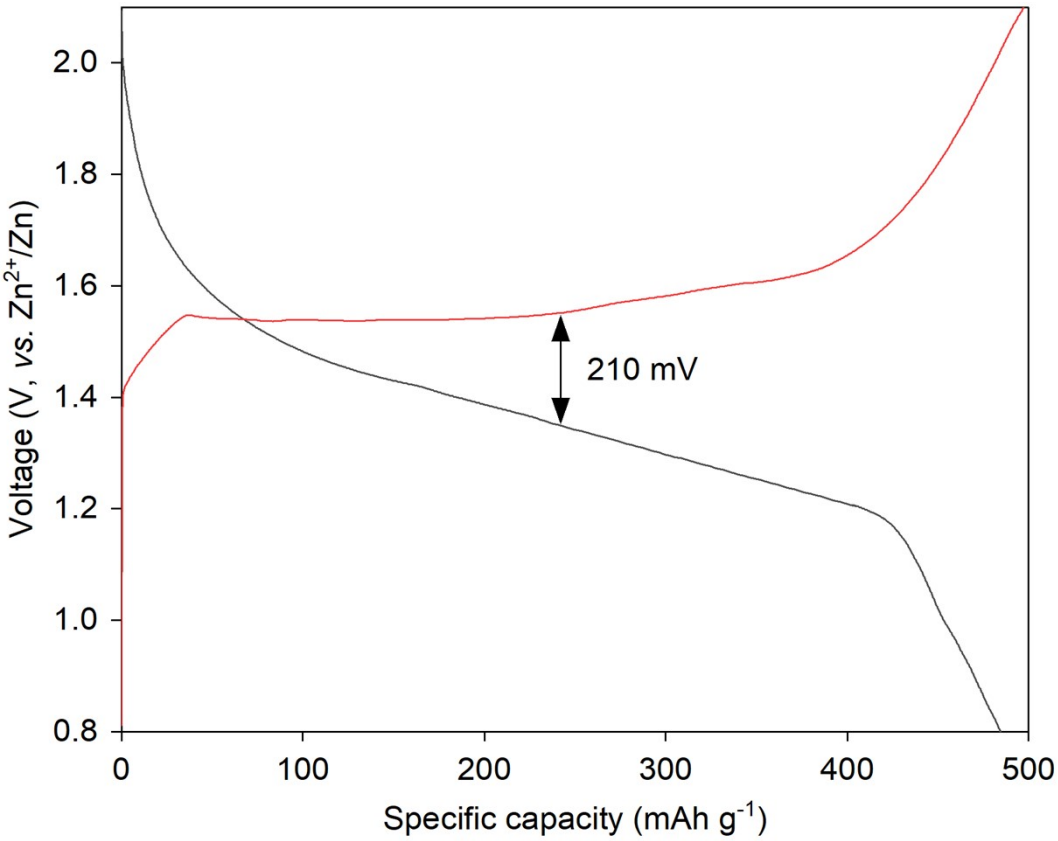

Figure S8: Charge discharge curve of ZMC-16 at a current rate of 50 mA g^{-1} with polarization voltage of 210 mV

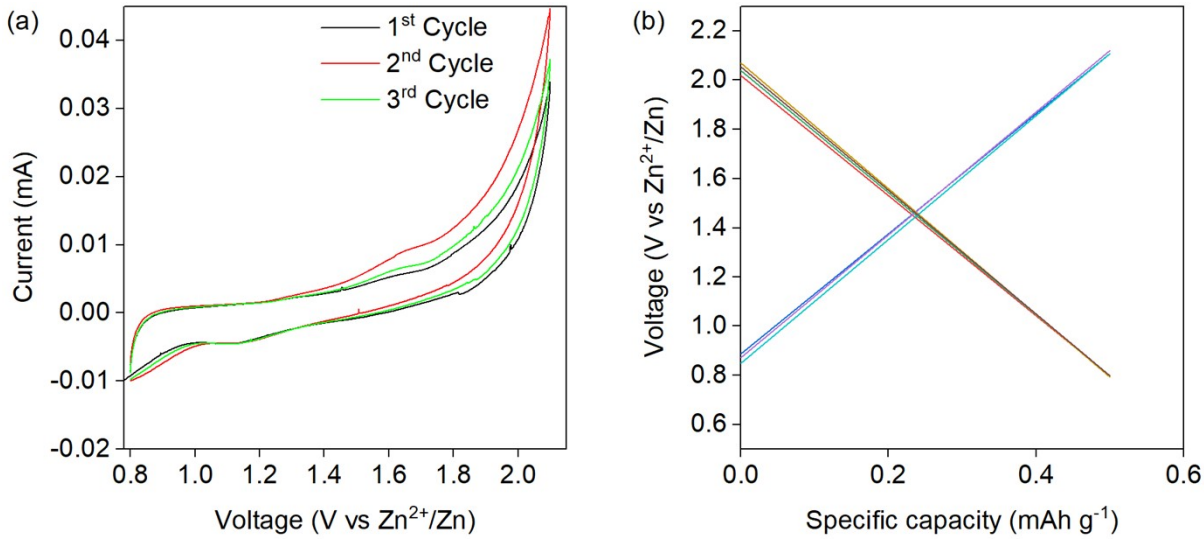

Figure S9. (a) CV curve of bare carbon cloth (CC) at 1 mV s^{-1}. (b) GCD profile of bare CC at 50 mA g^{-1}. Indicating no capacity contributions by CC

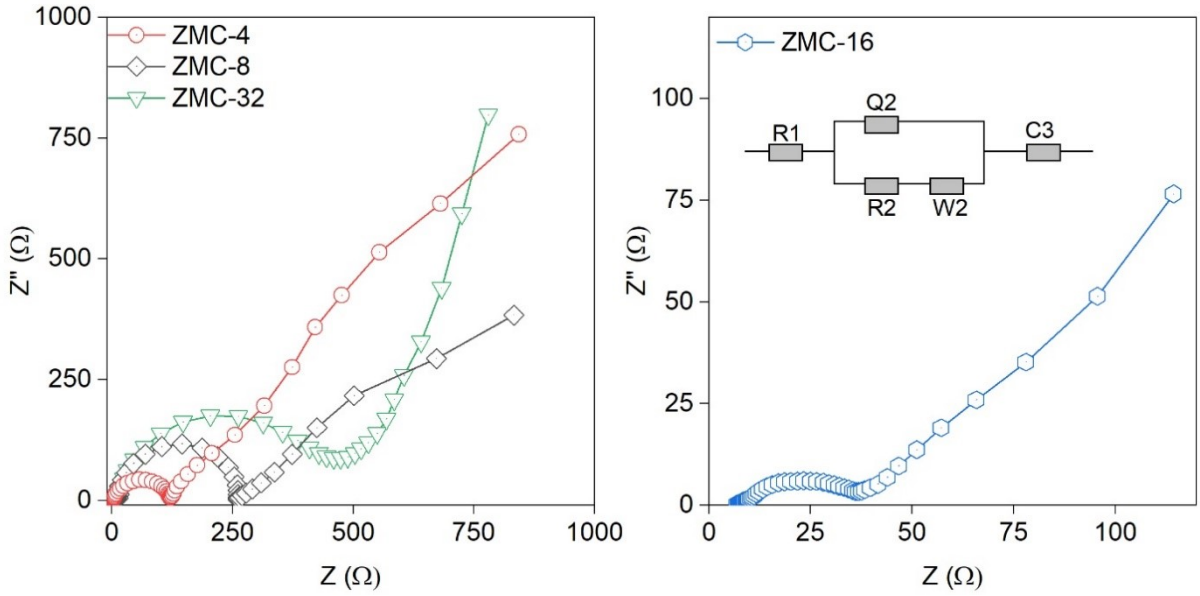

Figure S10: EIS was performed within the frequency range of 1 mHz to 1 MHz at 10 mV s^{-1}.

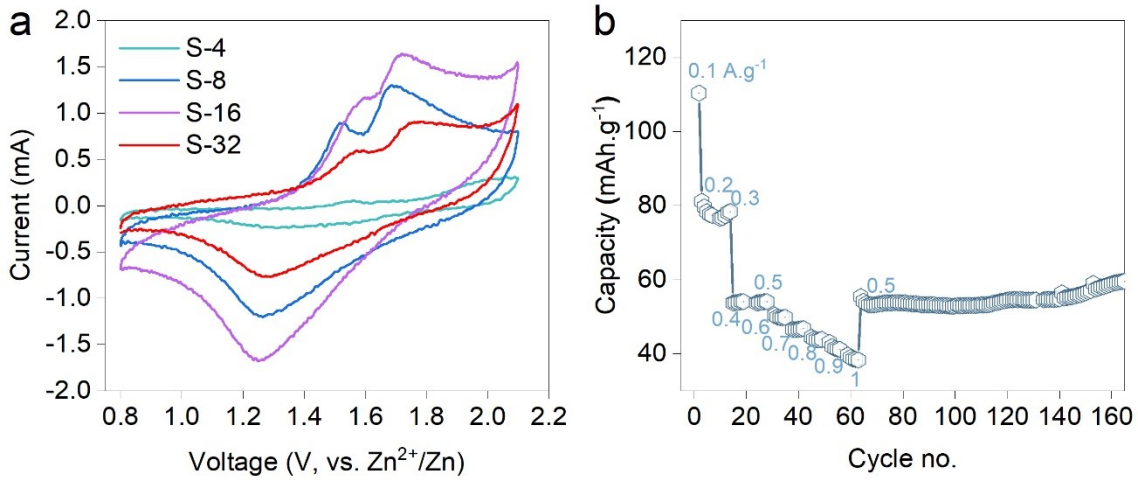

Figure S11. CV and rate capability of electrodeposited material prior to any heat treatment (a) CV curve of S-4/8/16/32 at a scan rate of 5 mV s^{-1}. (b) Rate capability test of S1600 at a different current rate ranging from 0.1 A g^{-1} to 1 A g^{-1}.

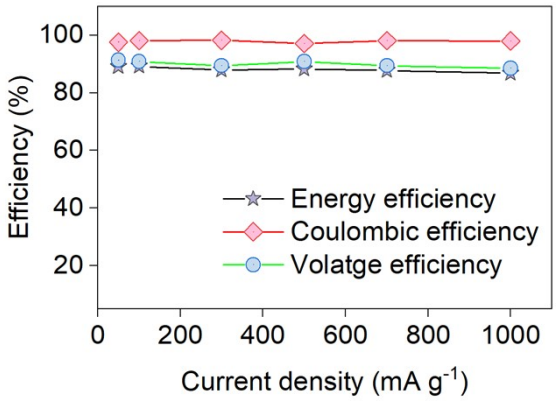

Figure S12. Energy, columbic, and voltage efficiency are plotted for various current densities.

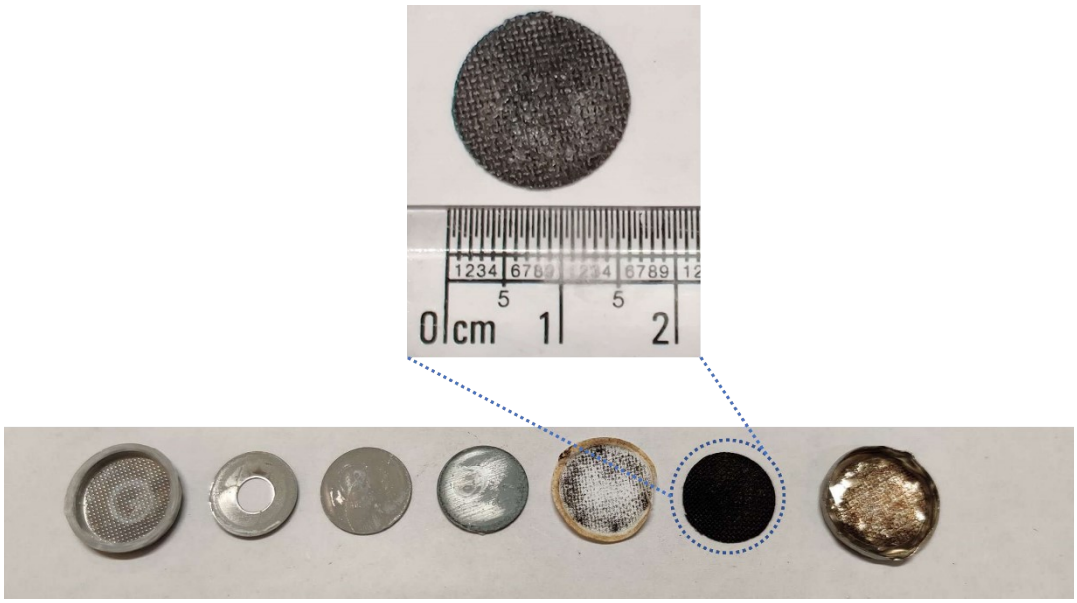

Figure S13. Coin cell de-crimped after 1000 cycles. (left to right) Negative casing, spring, spacer, metallic zinc (anode), separator, ZMC (cathode), and positive casing.

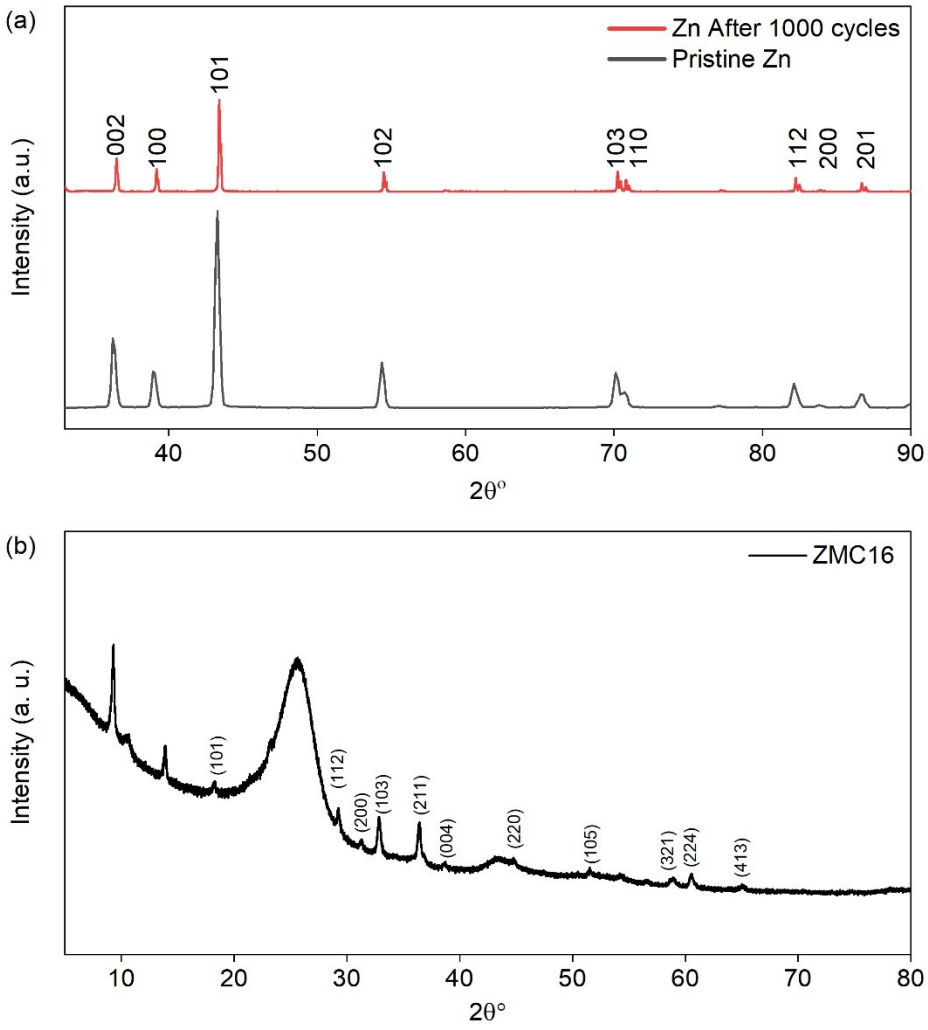

Figure S14. XRD pattern of anode and cathode after 1000 cycles. (a) The anode zinc foil of pristine and after 1000 cycles. (b) The cathode ZMC-16 cycled for 100 cycles.

Note S1

Energy density and power density calculation:

The specific capacity (mAh g^{-1}) is calculated according to the equation[1]:

$$C = \frac{\int_0^{\Delta t} i \times dt}{m} \quad \ldots (1)$$

where i (mA) is the applied discharging current, *Δt* (h) is the discharging time, and m

(g) is the mass loading of active material.

The specific energy density (W h kg^{-1}) E and specific power (W kg^{-1}) P are estimated based on the formulas:

$$E = \frac{\int_0^{\Delta t} V \times i}{m} dt \quad \ldots (2)$$

And $$P = \frac{E}{t} \quad \ldots (3)$$

where C is the specific capacity from equation (1), V is the working voltage window (0.8-2.1V) and t(h) discharging time of the assembled batteries.

Coulombic Efficiency, Energy Efficiency and Voltage Efficiency

To measure the reversibility of redox reaction coulombic efficiency (C.E.) and Energy efficiency (EE) is calculated as[2]:

$$CE = \frac{\int_0^{\Delta t} i_d dt}{\int_0^{\Delta t} i_c dt} \quad \ldots (4)$$

$$EE = \frac{\int_0^{\Delta t} V_d i_d dt}{\int_0^{\Delta t} V_c i_c dt} \quad \ldots (5)$$

Here, i_c and i_d is current during charge and discharge, V_c and V_d are volatge during charge and discharge, Δt is the time required for charge and discharge.

The voltage efficiency (VE) relation can be stated as

$$VE\ (\%) = \frac{EE}{CE} \quad \ldots (6)$$

NOTE S2

The reaction kinetics can be explained by Dunn's method, which provides information about diffusion-controlled processes. The current calculated from this method is[3]:

$$i = av^b \quad \ldots(1)$$

$$I\,(v) = k_1\,(v)^{0.5} + \; k_2\,v \quad \ldots(2)$$

$$\frac{I\,(v)}{v^{0.5}} = \; k_1 + \; k_2 v^{0.5} \quad \ldots(3)$$

Where I (v) ∝ ν, $k_1\,v$ = capacitive current

I (v) ∝ $\nu^{0.5}$, $k_1\,\nu^{0.5}$ = Diffusion-controlled current.

Where k_1, k_2, and are intercept, slope, and scan rates for ZMC-16 at different scan rates (0.2-1 $mV.s^{-1}$)

In addition, the Galvanostatic Intermittent Titration Technique (GITT) was used to quantify the ions' diffusion coefficients, which were then estimated using equation (4), shown below.

The formula for determining GITT using *Fick's second law*[4]*:*

$$D = \frac{4L^2}{\pi\tau}\left(\frac{\Delta E_s}{\Delta E_\tau}\right)^2 \quad \ldots(4)$$

Here, the duration of the current pulse (s) is represented by t, τ is the relaxation time (s), and ΔE_s represent the steady-state potential change (V) by the current pulse. ΔE_t is the potential change (V) during the constant current pulse after eliminating the iR drop. L is the ion diffusion distance (cm), and the electrode thickness is often used to express its value.

Table S1: Detailed comparison of recently reported non aqueous and aqueous ZIB.

S. No.	Cathode||Anode	Electrolyte	Capacity (mAh g^{-1}) @ Rate (mA g^{-1})	Energy density (Wh Kg^{-1})	Power (W Kg^{-1})	Cycle life Performance (Retention% of initial discharge capacity mAh g^{-1} after cycles at current rate mA g^{-1})	Voltage Window (V)	Ref.
			Non-aqueous electrolytes					
1	δ-MnO_2||Zn	0.25 M $(CF_3SO_3)_2Zn$ DMSO	159 @ 50	175	56	60% of 159 mAh g^{-1} after 900 cycles at 6000 mA g^{-1}	0.75-1.8	5
2	$K_{0.86}Ni[Fe(CN)_6]_{0.954}(H_2O)_{0.766}$||Zn	0.5 M $Zn(ClO_4)_2$ ACN	55.6 @ 11.2	-	-	90% of 55.6 mAh g^{-1}after 35 cycles at 11.2 mA g^{-1}	0.7-1.8	6
3	$V_3O_7.H_2O$	0.25 M $Zn(CF_3SO_3)_2$ ACN	59 @ 5	-	-	-	0.5-1.8	7
4	δ-MnO_2||Zn	0.5 M $Zn(TFSI)_2$ ACN	123 @ 12.3	-	-	60% of 95 mAh g^{-1}after 125 cycles at 12.3 mA g^{-1}	0.05-1.9	8
5	V_2O_5||Zn	0.5 M $Zn(TFSI)_2$ ACN	196 @ 14.4	144	1500	> 90% of 164 mAh g^{-1} after 120 cycles at 14.4 mA g^{-1}	0.3-1.5	9
6	$Na_2Mn[Fe(CN)_6]$||Zn	0.5 M $Zn(CF_3SO_3)_2$ + 1M NaFSI in TMP	89.3 @ 160	-	-	77% of 89.3 mAh g^{-1} after 1000 cycles at 160 mA g^{-1}	1-2.2	10

7	Graphite||Zn	1 M $(Zn(TFSI)_2$ ACN	53 @ 50	86.5	4400	97.3% of 42.7 mAh g^{-1} after 1000 cycles at 1000 mA g^{-1}	1-2.55	[11]
8	$ZnAl_xCo_{2-x}O_4$||Zn	0.3 M $Zn(CF_3SO_3)_2$ in MeCN	134 @ 32	-	-	>75% of 134 mAh g^{-1} after 1000 cycles at 1000 mA g^{-1}	1.4-2.15	[12]
9	$Na_3V_2(PO_4)_3$||Zn	1 M $NaCF_3SO_4$ + 0.1 M $Zn(CF_3SO_3)_2$ in TEP	84 @ 500	-	-	100% of 84 mAh g^{-1} after 600 cycles at 500 mA g^{-1}	0.6-1.9	[13]
10	$Na_3V_2(PO_4)_2O_2F$ ||Zn	0.5 M $Zn(CF_3SO_3)_2$ + 1 M $NaClO_4$ in TMP	113 @ 130	203	-	83.5% of 113 mAh g^{-1} after 1000 cycles at 130 mA g^{-1}	0.8–2.4	[14]
11	Sodium vanadate (NVO)||Zn	0.5 M $ZnCl_2$-ethaline DES	310 @ 100	282	90	68% of 244 mAh g^{-1} after 300 cycles at 300 mA g^{-1}	0.01-1.8	[15]
12	$Zn_xMo_{2.5+y}VO_{9+z}$||Zn	0.2 M $Zn(CF_3SO_3)_2$ in(PC)/ (DMSO) (1 : 4)	220 @ 20	-	-	77% of 220 mAh g^{-1} after 35 cycles at 2 mA g^{-1}	0.01-1.7	[16]
13	$ZnNi_{1/2}Mn_{1/2}CoO_4$||Zn	0.3 M $Zn(CF_3SO_3)_2$ +200 ppm (DABCO) in MeCN	180 @ 42	305	-	81% of 180 mAh g^{-1} after 200 cycles at 42 mA g^{-1}	0.8-2.15	[17]
14	3D-NRAs-	1 M $Zn(ClO4)_2$	336 @ 50	-	-	85% of 207 mAh g^{-1} after	0.4–1.6	[18]

	V_2O_5||Zn	PC				5000 cycles at 10000 mA g^{-1}		
				Aqueous electrolytes				
15	$V_3O_7H_2O$ ||Zn	1 M $ZnSO_4$	325 @ 1500	240	-	80% of 275 mAh g^{-1}after 200 cycles at 3000 mA g^{-1}	0.4-1.1	[7]
16	MnVO||Zn	3 M $Zn(CF_3SO_3)_2$	415 @ 50	267	5791	92% of 260 mAh g^{-1}after 2000 cycles at 4000 mA g^{-1}	0.2-1.6	[19]
17	$Zn_3V_2O_7(OH)_2 \cdot 2H_2O$||Zn	1 M $ZnSO_4$	213 @ 50	214	-	68% of 150 mAh g^{-1}after 300 cycles at 200 mA g^{-1}	0.2-1.8	[20]
18	$ZnMn_2O_4$||Zn	1 M $ZnSO_4$+ 0.1M $MnSO_4$	172 @ 100	303	-	79% of ≈ 62 mAh g^{-1}after 1000 cycles at 2000 mA g^{-1}	0.6 -1.9	[21]
19	$ZnMn_2O_4$/C||Zn	3 M $Zn(CF_3SO_3)_2$	150 @ 50	202	-	94% of ≈ 90 mAh g^{-1}after 500 cycles at 500 mA g^{-1}	0.8-1.9	[22]
20	P–$NiCo_2O_{4-x}$||Zn	1 M KOH + 0.05M $Zn(ac)_2$	365.8 @ 3000	616.5	5150	73.8% of 365.8 mAh g^{-1} after 5000 cycles at 3000 mA g^{-1}	1.4-1.9	[23]
21	$ZnMn_2O_4$||Zn	1 M $ZnSO_4$ +0.05M $MnSO_4$	134.7 @ 100	-	-	59.2% of 86 mAh g^{-1}after 300 cycles at 100mA g^{-1}	0.8–1.9	[24]
22	PANI||Zn	1 M $Zn(CF_3SO_3)_2$	191 @ 50	-	-	92% of 82 mAh g^{-1}after 3000 cycles at 5000mA g^{-1}	0.5–1.5	[25]
23	V_2O_5@ PEDOT||Zn	2.5 M $Zn(CF_3SO_3)_2$	360 @100	-	-	97% of 360 mAh g^{-1}after 600 cycles at 1000 mA g^{-1}	0.2-1.6	[26]
24	$NaV_3O_8 \cdot 1.5H_2O$ (NVO)||Zn	1 M $ZnSO_4$/1 M Na_2SO_4	380 @ 50	300	86	82% of 165 mAh g^{-1} after1000 at 4000 mA g^{-1}	0.3–1.25	[27]
25	$Na_{0.33}V_2O$ ||Zn	3 M $Zn(CF_3SO_3)_2$	367.1 @ 100	-	-	93% of 218 mAh g^{-1} after1000 cycles at 1000 mA	0.2-1.6	[28]

						g^{-1}		
26	**ZMC||Zn**	**0.5 M $Zn(ClO_4)_2$ in ACN**	**469 @ 50**	**632**	**70**	**88 % of 152 mAh g^{-1} after 1000 cycles at 1000 mA g^{-1}**	**0.8-2.1**	**This work**

DMSO: Dimethyl sulfoxide; MeCN/ACN: Acetonitrile; TMP: Trimethyl phosphate; TEP: Triethyl phosphate; PC: propylene carbonate; DES: Deep eutectic solvents; DABCO: 1,4-diazabicyclo[2.2.2]octane.

References:

1 Y. Shen, Z. Li, Z. Cui, K. Zhang, R. Zou, F. Yang and K. Xu, J. Mater. Chem. A, 2020, 8, 21044–21052.

2 P. Meister, H. Jia, J. Li, R. Kloepsch, M. Winter and T. Placke, Chem. Mater. 2016, 28, 7203–7217.

3 Y. Liu, C. Li, J. Xu, M. Ou, C. Fang, S. Sun, Y. Qiu, J. Peng, G. Lu, Q. Li, J. Han and Y. Huang, Nano Energy, 2020, 67, 104211.

4 R. Li, H. Zhang, Q. Zheng and X. Li, J. Mater. Chem. A, 2020, 8, 5186–5193.

5 W. Kao-ian, M. T. Nguyen, T. Yonezawa, R. Pornprasertsuk, J. Qin, S. Siwamogsatham and S. Kheawhom, Mater. Today Energy, 2021, 21, 100738.

6 M. S. Chae, J. W. Heo, H. H. Kwak, H. Lee and S. T. Hong, J. Power Sources, 2017, 337, 204–211.

7 D. Kundu, S. Hosseini Vajargah, L. Wan, B. Adams, D. Prendergast and L. F. Nazar, Energy Environ. Sci., 2018, 11, 881–892.

8 S. D. Han, S. Kim, D. Li, V. Petkov, H. D. Yoo, P. J. Phillips, H. Wang, J. J. Kim, K. L. More, B. Key, R. F. Klie, J. Cabana, V. R. Stamenkovic, T. T. Fister, N. M. Markovic, A. K. Burrell, S. Tepavcevic and J. T. Vaughey, Chem. Mater., 2017, 29, 4874–4884.

9 P. Senguttuvan, S. Han, S. Kim, A. L. Lipson, S. Tepavcevic, T. T. Fister, I. D. Bloom, A. K. Burrell and C. S. Johnson, Adv. Energy Mater., 2016, 6, 1600826.

10 A. Naveed, J. Chen, B. Raza, Y. Liu and J. Wang, J. Electroanal. Chem., 2022, 904, 115949.

11 N. Zhang, Y. Dong, Y. Wang, Y. Wang, J. Li, J. Xu, Y. Liu, L. Jiao and F. Cheng, ACS Appl. Mater. Interfaces, 2019, 11, 32978–32986.

12 C. Pan, R. G. Nuzzo and A. A. Gewirth, Chem. Mater., 2017, 29, 9351–9359.

13 Q. Li, K. Ma, C. Hong, G. Yang and C. Wang, Sci. China Mater., 2021, 64, 1386–1395.

14 Y. Dong, S. Di, F. Zhang, X. Bian, Y. Wang, J. Xu, L. Wang, F. Cheng and N. Zhang, J. Mater. Chem. A, 2020, 8, 3252–3261.

15 S. C. Wu, M. C. Tsa, H. J. Liao, T. Y. Su, S. Y. Tang, C. W. Chen, H. A. Lo, T. Y. Yang, K. Wang, Y. Ai, Y. Z. Chen, L. Lee, J. F. Lee, C. J. Lin, B. J. Hwang and Y. L. Chueh, ACS Appl. Mater. Interfaces, 2022, 14, 7814–7825.

16 W. Kaveevivitchai and A. Manthiram, J. Mater. Chem. A, 2016, 4, 18737–18741.

17 C. Pan, R. Zhang, R. G. Nuzzo and A. A. Gewirth, Adv. Energy Mater., 2018, 8, 1800589.

18 D. Chen, X. Rui, Q. Zhang, H. Geng, L. Gan, W. Zhang, C. Li, S. Huang and Y. Yu, Nano Energy, 2019, 60, 171–178.

19 C. Liu, Z. Neale, J. Zheng, X. Jia, J. Huang, M. Yan, M. Tian, M. Wang, J. Yang and G. Cao, Energy Environ. Sci., 2019, 12, 2273–2285.

20 C. Xia, J. Guo, Y. Lei, H. Liang, C. Zhao and H. N. Alshareef, Adv. Mater., 2018, 30, 1705580.

21 V. Soundharrajan, B. Sambandam, S. Kim, S. Islam, J. Jo, S. Kim, V. Mathew, Y. Sun and J. Kim, Energy Storage Mater., 2020, 28, 407–417.

22 N. Zhang, F. Cheng, Y. Liu, Q. Zhao, K. Lei, C. Chen, X. Liu and J. Chen, J. Am. Chem. Soc., 2016, 138, 12894–12901.

23 Y. Zeng, Z. Lai, Y. Han, H. Zhang, S. Xie and X. Lu, Adv. Mater., 2018, 30, 1802396.

24 X. Wu, Y. Xiang, Q. Peng, X. Wu, Y. Li, F. Tang, R. Song, Z. Liu, Z. He and X. Wu, J. Mater. Chem. A, 2017, 5, 17990–17997.

25 F. Wan, L. Zhang, X. Wang, S. Bi, Z. Niu and J. Chen, Adv. Funct. Mater., 2018, 28, 1804975.

26 D. Xu, H. Wang, F. Li, Z. Guan, R. Wang, B. He, Y. Gong and X. Hu, Adv. Mater. Interfaces, 2019, 6, 1801506.

27 F. Wan, L. Zhang, X. Dai, X. Wang, Z. Niu and J. Chen, Nat. Commun., 2018, 9, 1656.

28 P. He, G. Zhang, X. Liao, M. Yan, X. Xu, Q. An, J. Liu and L. Mai, Adv. Energy Mater., 2018, 8, 1702463.